Comput Geosci (2009) 13:43–55
DOI 10.1007/s10596-008-9104-z

ORIGINAL PAPER

Unraveling reservoir compaction parameters through the inversion of surface subsidence observations

A. G. Muntendam-Bos · P. A. Fokker

Received: 11 February 2008 / Accepted: 7 August 2008 / Published online: 6 September 2008

Abstract In an attempt to derive more information on the parameters driving compaction, this paper explores the feasibility of a method utilizing data on compaction-induced subsidence. We commence by using a Bayesian inversion scheme to infer the reservoir compaction from subsidence observations. The method's strength is that it incorporates all the spatial and temporal correlations imposed by the geology and reservoir data. Subsequently, the contributions of the driving parameters are unravelled. We apply the approach to a synthetic model of an upscaled gas field in the northern Netherlands. We find that the inversion procedure leads to coupling between the driving parameters, as it does not discriminate between the individual contributions to the compaction. The provisional assessment of the parameter values shows that, in order to identify adequate estimate ranges for the driving parameters, a proper parameter estimation procedure (Markov Chain Monte Carlo, data assimilation) is necessary.

Keywords Subsidence · Compaction · Delay · Covariance · Inversion

1 Introduction

Most producing hydrocarbon reservoirs undergo compaction, which may result in improved recovery but is also responsible for a number of field operating problems. In addition, the compaction is usually accompanied by land subsidence. Since it can alter the economics of field development and has significant social repercussions (e.g., possible damage to buildings and infrastructure), it is important for both the operator and the stakeholders to be able to predict and monitor the amount of reservoir compaction.

The relationship between reservoir compaction and surface subsidence can be exploited in modeling. If the degree of compaction is known, or can be predicted to an acceptable level of confidence, the actual or expected subsidence can be estimated by forward modeling [1–10]. Inverse modeling is required to obtain knowledge about or confirmation of subsurface processes from surface measurements [11–17].

Muntendam-Bos et al. [18] recently introduced an inversion scheme that utilizes all available geological information to derive a time-dependent model estimate for the reservoir compaction. The method uses both the prior model covariance matrix and the data covariance matrix, which incorporate the spatial and temporal correlations between model parameters and data, respectively. The incorporation of the model covariance implicitly guarantees a realistic smoothness of the inverted model, while maintaining specific geological features, such as sharp boundaries. Taking these relationships into account through the model covariance matrix enhances the influence of the data on the inverted model estimate. Therefore, unlike more common inversion procedures, this method is able to properly resolve the characteristics of dynamic reservoir compaction (see [18] for details).

The synthetic model that Muntendam-Bos et al. [18] use as an example takes only one uncertain parameter (the transmissibility of the free water level) into

A. G. Muntendam-Bos (✉) · P. A. Fokker
TNO Built Environment and Geosciences -
Geological Survey of the Netherlands,
Postbus 80015, 3508 TA Utrecht, The Netherlands
e-mail: annemarie.muntendam@tno.nl

account, thus assuming that all other parameters are perfectly known. In order to apply the procedure to real field cases, the behavior of the inversion procedure with respect to multiple uncertain parameters needs to be evaluated. The goal of the present paper is to demonstrate the feasibility of utilizing the reservoir compaction model inferred from subsidence information to distinguish the characteristics of several compaction-driving parameters.

The forward models mentioned above all assume that subsidence responds instantly to reservoir compaction. In turn, compaction is normally assumed to be linearly correlated with the decrease in reservoir pressure, i.e., the compaction coefficient is constant. However, in sandstones, subsidence can show a nonlinear dependence on reservoir pore pressure. This nonlinearity in subsidence response may be seen as a shift between the start of depletion and the (delayed) start of subsidence [19], or as an increase in subsidence rate with time. This time lag in subsidence response has been observed for several oil and gas fields (e.g., Bachaquero [19–21], Tia Juana [19, 22], the SNOK field [23], and Wilmington [21, 24]). The underlying cause of the time lag has been attributed to mechanisms related to reservoir compaction (such as creep, an intrinsic rate effect, and an elastic–plastic transition, [19]). Alternatively, the nonlinearity of the subsidence response is attributable to the compaction coefficient being dependent on depletion: hence, the gradual response in reservoir compaction. De Waal and Smits [21] have developed a model on the basis of extensive laboratory studies. The model was derived from a theory relating compaction to time-dependent intergranular friction and explains both field and laboratory compaction behavior by one single normalized, nonlinear compaction curve. This nonlinear compaction curve can be described by a linear dependence of the compaction coefficient on the pressure depletion of the reservoir:

$$c_m(dP) = a \cdot dP + b \tag{1}$$

with a the slope (in bar^{-2}) and b the y-intercept (in bar^{-1}) of the linear relationship. The depletion dP is measured in bar.

In this paper, we extend the synthetic model of Muntendam-Bos et al. [18] by introducing a significantly uncertain compaction coefficient for the reservoir sandstone. This compaction coefficient is allowed either to be constant with respect to the reservoir pressure depletion or to be linearly dependent on the pressure depletion. Our analysis consists of two consecutive procedures. We commence by deriving the reservoir compaction field through a Bayesian inversion of subsidence observations. Subsequently, a simple, crude procedure is used to unravel the uncertain compaction-driving parameters. This two-step scheme allows us to ascertain whether our inversion procedure is capable of identifying depletion-dependent behavior of the compaction coefficient, while at the same time resolving the uncertain transmissibility of the free water level.

In the next section, we give a brief overview of the method. This is followed by a description of the synthetic reservoir model we utilize. Then, the inversion results are presented, the dynamic reservoir parameters are unraveled, and the results are discussed. Finally, conclusions are drawn.

2 Methodology

2.1 Compaction inversion procedure

The exploitation of hydrocarbons induces ground or seabed subsidence due to the reduction of pressure in the reservoir. The pressure changes affect the in situ stress field through poro-elastic coupling, causing the reservoir to compact and the surface to subside. Due to the elastic properties of the overburden, the compaction in the reservoir is transferred to the surface almost instantaneously. However, the subsidence extends over a wider area than the reservoir compaction. The area affected is roughly as extensive as the reservoir depth. The precise form of the subsidence bowl resulting from the reservoir compaction depends on the properties of the subsurface.

For the forward model, we use a linear, semianalytic approach designed to account for layering [10]. The method combines a number of analytic functions that satisfy the elasticity equations in such a way that the boundary conditions at layer interfaces and the ground surface are approximated (see [10] for details). The solution obtained by this method yields a subsidence bowl originating from a center of compression, which is the mathematical representation of a finite amount of compaction concentrated at a single point. This solution is subsequently used as an influence function or Green function in conjunction with the reservoir data to arrive at a subsidence bowl for the whole reservoir that is compacting. Because the reservoir pressures available from reservoir simulations are on discretized models, the total predicted subsidence resulting from reservoir

compaction at a surface location is obtained by summation over all grid blocks in the reservoir:

$$u_3(x_i, y_i) = \sum_j c_{m_j} \cdot \delta V_j \cdot \delta P_j \cdot g\left(\sqrt{(x_i - x_j)^2 + (y_i - y_j)^2}\right) \quad (2)$$

In this equation, $g(r)$ indicates the influence function for vertical displacement at the surface, δV_j is the volume of the j-th grid block, δP_j is the pressure depletion in this grid block, and c_{m_j} is the compaction coefficient, which may be dependent on the grid block depletion (dP_j).

For a set of subsidence observations, Eq. 2 yields a linear, coupled system of equations represented by $\mathbf{Gm} = \mathbf{d}$, where $G_{ij} = g(r_{ij}) = g(\sqrt{(x_i - x_j)^2 + (y_i - y_j)^2})$ is the coefficient matrix relating the subsidence observations ($d_i = u_3(x_i, y_i)$), gathered in the data vector $\mathbf{d}$, to the model parameters ($m_j = c_{m_j} \cdot \delta V_j \cdot \delta P_j$), gathered in the vector $\mathbf{m}$. Some of the uncertain properties of the forward model, such as an unknown global bias in the subsidence measurements (unstable reference level), can also be incorporated into the model vector $\mathbf{m}$ [25].

The formal least-squares solution of our system is [18]:

$$\mathbf{m} = \mathbf{m}_0 + \mathbf{C}_m\mathbf{G}^T(\mathbf{G}\mathbf{C}_m\mathbf{G}^T + \mathbf{C}_d)^{-1}(\mathbf{d} - \mathbf{G}\mathbf{m}_0) \quad (3)$$

where $\mathbf{m}_0$ is the prior model and $\mathbf{C}_d$ and $\mathbf{C}_m$ denote the data and prior model covariance matrices, respectively. The diagonal elements of these matrices comprise the squared errors on the data and model parameters. If the relationships in space and time are absent, the off-diagonal elements of the covariance matrices will be zero. The superscript T denotes the transposed. The corresponding posterior covariance is given by $\mathbf{C} = \mathbf{C}_m - \mathbf{C}_m\mathbf{G}^T(\mathbf{G}\mathbf{C}_m\mathbf{G}^T + \mathbf{C}_d)^{-1}\mathbf{G}\mathbf{C}_m$ and the model resolution kernel is $\mathbf{R} = \mathbf{C}_m\mathbf{G}^T(\mathbf{G}\mathbf{C}_m\mathbf{G}^T + \mathbf{C}_d)^{-1}\mathbf{G}$ (see [26] for more details).

The result of the inversion is now dependent on the prior information: the prior model ($\mathbf{m}_0$) and the prior model covariance matrix ($\mathbf{C}_m$). The nonzero covariance in $\mathbf{C}_m$ quantifies the expected relationships between grid points in space and time [18]. Such knowledge is often available, even when the absolute values of the initial compaction models are uncertain.

The temporal aspect of the problem is implicit in Eq. 3. In order to ensure that all the available measured data are used optimally, the method has been extended to deal with measurement stations that are not included in every campaign (see [18] for details). Basically, for each site omitted from one or more observation campaigns, the difference between the measurements in the campaign following the omission and the campaign preceding the omission is related to all the intermediate models.

2.2 Unraveling compaction-driving parameters

In addition to achieving the inversion of the subsidence information to compaction, our aim in this paper is to derive estimates for the uncertain compaction-driving parameters. This is a nonlinear inversion in itself, which cannot be linearized. Therefore, the best approach would be to adopt data assimilation (e.g., ensemble Kalman filter), neighborhood algorithm, or Markov chain Monte Carlo techniques. These techniques can obtain well-defined estimates and error ranges of the driving parameters. However, they require an integrated system of reservoir simulation and surface subsidence inversion and create a range of new challenges. Given that our objective is to demonstrate the feasibility of utilizing the compaction inferred from subsidence data to distinguish the characteristics of the driving parameters, such a fully integrated system is beyond the scope of the present paper. We have therefore adopted a simple, somewhat crude approach to derive estimates and error ranges of the uncertain parameters. These estimates are subsequently verified for compliance with the inferred reservoir compaction field. Since this approach is specific for the characteristics of the particular synthetic case used, the details of the procedure will be explained during the application in Section 4.2.

3 Synthetic case study

We have applied the above mentioned method to a synthetic case, representing an upscaled gas field in the northern Netherlands (Fig. 1; for the characteristics of the synthetic reservoir, see Table 1). By focussing on a synthetic case, a proper comparison between the inverted and "true" model and driving parameter values can be obtained. The prior model ($\mathbf{m}_0$) and model covariance ($\mathbf{C}_m$) are obtained in the same way as in a real case [27]: the available geological information (i.e., size and depth of the reservoir, shape, presence of faults, permeability, porosity, saturation) and, in this case, the uncertainties in the transmissibility of the gas/water interface, and the compaction coefficient (see Table 2) are combined with the production information (i.e., production profiles) in a Monte Carlo study using

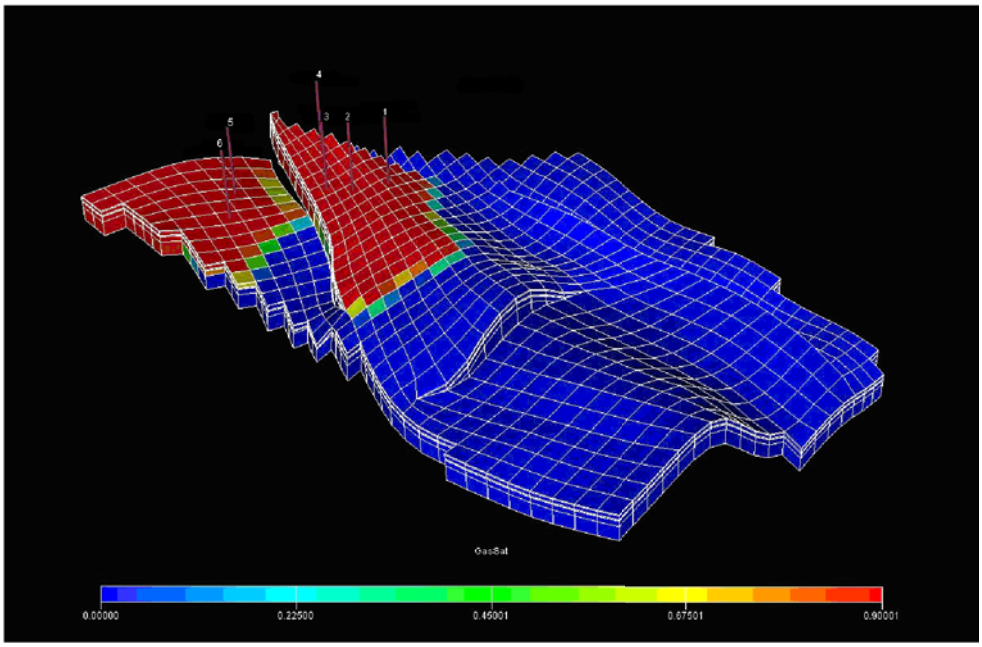

Fig. 1 Reservoir model indicating gas (*red*) and water saturation (*blue*). The reservoir is cut by three nearly vertical faults and has a transmissibility across the gas/water interface of 0.0337. The compaction of the reservoir sandstone is linearly dependent on the depletion ($C_m(dP) = (0.0022 \cdot dP + 0.2) \cdot 10^{-5}$ bar^{-1}). The reservoir is located at a depth of 2,300 m and has a constant thickness of 182 m. The reservoir is depleted by six wells (shown in the figure)

Table 1 Characteristics of the synthetic reservoir

Description	Value
Depth	2,300 m
Surface area	$22.19 \cdot 10^6$ m^2
Thickness	182 m
Number of layers	6
Number of faults	3
Depletion period	15 years
Average total pressure drop	180 bar
Depletion-dependent compaction coefficient	$(0.0022 \cdot 10^{-5} \cdot dP + 0.2 \cdot 10^{-5})$ bar^{-1}
Transmissibility gas/water interface[a]	0.0337
Thickness of overlying salt layer	600 m

[a]This transmissibility is a permeability multiplier controlling the response of the aquifer to gas depletion (i.e., a transmissibility of 0 results in no aquifer response to gas depletion, whereas $T = 1.0$ induces full aquifer support). A permeability multiplier induces a relative permeability effect once aquifer water enters the gas-bearing zone of the reservoir [29]

Table 2 Overview of the parameter values used in the Monte Carlo approach to derive the prior model covariance matrix

The compaction coefficient after 15 years of production has been computed with the maximum depletion after 15 years of 180 bars

T	c_m ($= (a \cdot dP + b) \cdot 10^{-5}$ bar^{-1})		
	a ($\cdot 10^{-5}$ bar^{-2})	b ($\cdot 10^{-5}$ bar^{-1})	c_m (bar^{-1}; after 15 years)
0.001	0	0.4425	0.4425
0.00245	0	0.7301	0.7301
0.0036	0.0008535	0.4	0.5545
0.0083	0.0011	0.3	0.4984
0.0149	0.0012	0.2	0.4168
0.0191	0.0017	0.4	0.706
0.0265	0.0018	0.1	0.4254
0.0444	0.002	0	0.3511
0.0556	0.0026	0.2	0.6699
0.1	0.0032	0	0.5819

a reservoir simulator. This way, a pressure depletion profile and covariance are generated for the reservoir, which are used as a prior in the inversion. The details of this procedure are given in the Appendix. The subsidence data **d** are generated by the forward model using the "true" geological input. A random error was added to every single data point in order to simulate errors in implicit assumptions. The size of the bandwidth around the true value was 0.005'm on the average; the bandwidth size was drawn from a Gaussian distribution with a mean of 0.005 m and a standard deviation of 0.002 m (see [18]).

4 Results

Given that our aim is to demonstrate the feasibility of utilizing the reservoir compaction model inferred from subsidence information to distinguish the characteristics of several compaction driving parameters, we need to perform the inversion exercise first, and then unravel the uncertain reservoir parameters from the inferred compaction field.

By means of the inversion exercise, we resolve the time-dependent compaction model using the full geological information, i.e., all correlations in space and time in the reservoir, depending on the transmissibility and compaction coefficient. The uncertain dynamic reservoir parameters that must be derived from the inverted model are the dependence of the compaction coefficient on the pressure depletion and the transmissibility of the model estimate.

4.1 Inversion model

In our inversion procedure, we estimate the compaction of the reservoir grid cells ($dV = c_m \cdot dP \cdot V$) from the subsidence information. The volume of each grid cell is a fixed parameter, so we will focus our analysis of the results on the dimensionless model $m_D = dV/V = c_m \cdot dP$. We compare the results of the inversion, i.e. the model estimate m_D^{est} with the prior and "true" dimensionless models, m_D^{prior} and m_D^{true}.

Figure 2 shows the m_D^{est} for the inverted model estimate at each time step. Figures 3 and 4 show the differences between the inverted model and the prior and "true" models, respectively. Compared to m_D^{prior}, the m_D^{est} of the gas-bearing part of the reservoir is smaller for the initial time steps (3, 6, and 9 years of production) and larger for the later time steps (12 and 15 years of production). For the aquifer, the m_D^{est} of the inverted model is larger than m_D^{prior} for all time steps. The differences by comparison with m_D^{true} are largest in the gas-bearing part of the reservoir. Here, the inverted

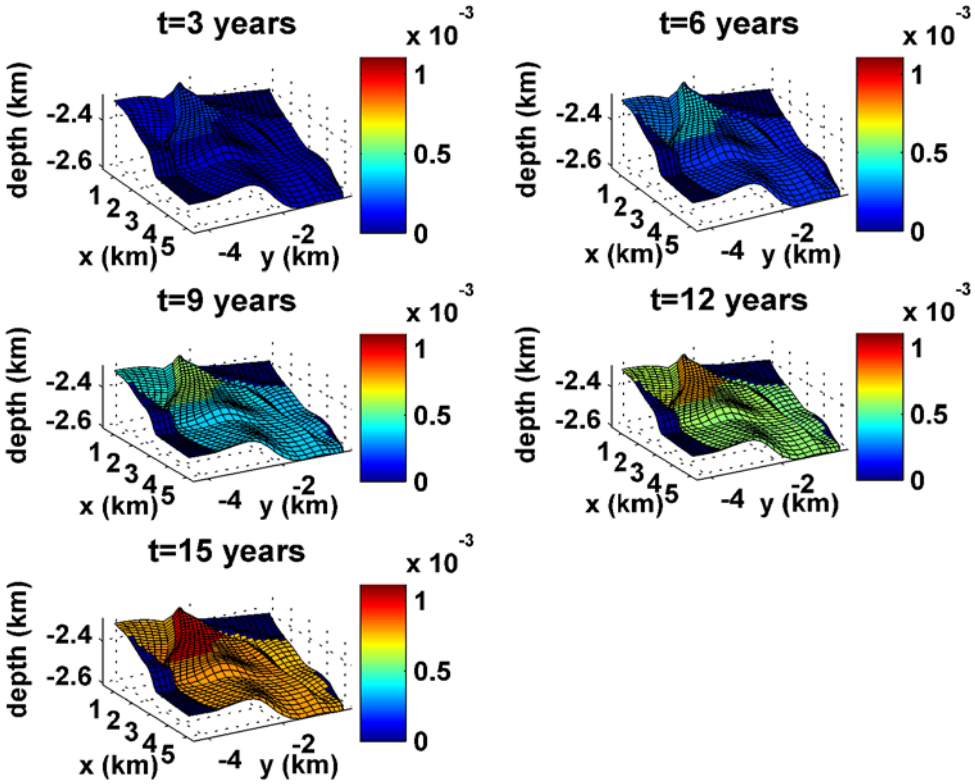

Fig. 2 Inverted estimate of the dimensionless model (m_D^{est})

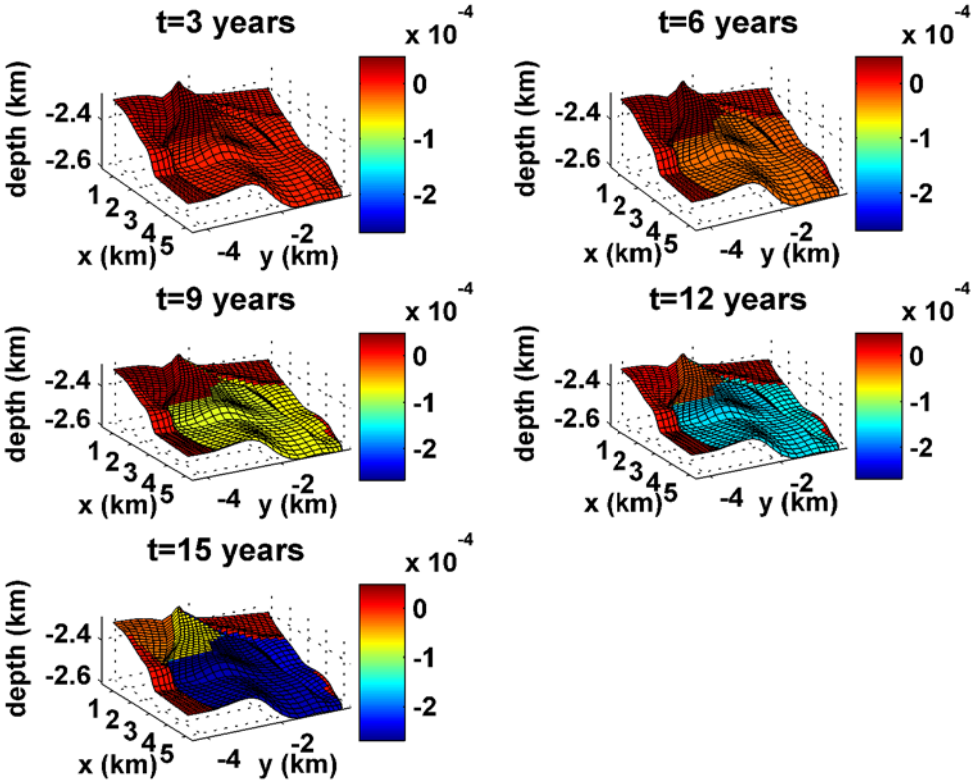

Fig. 3 Difference between the m_D^{prior} and m_D^{est}. Note that the main difference is concentrated in the aquifer part of the model (for full analysis, see the main text)

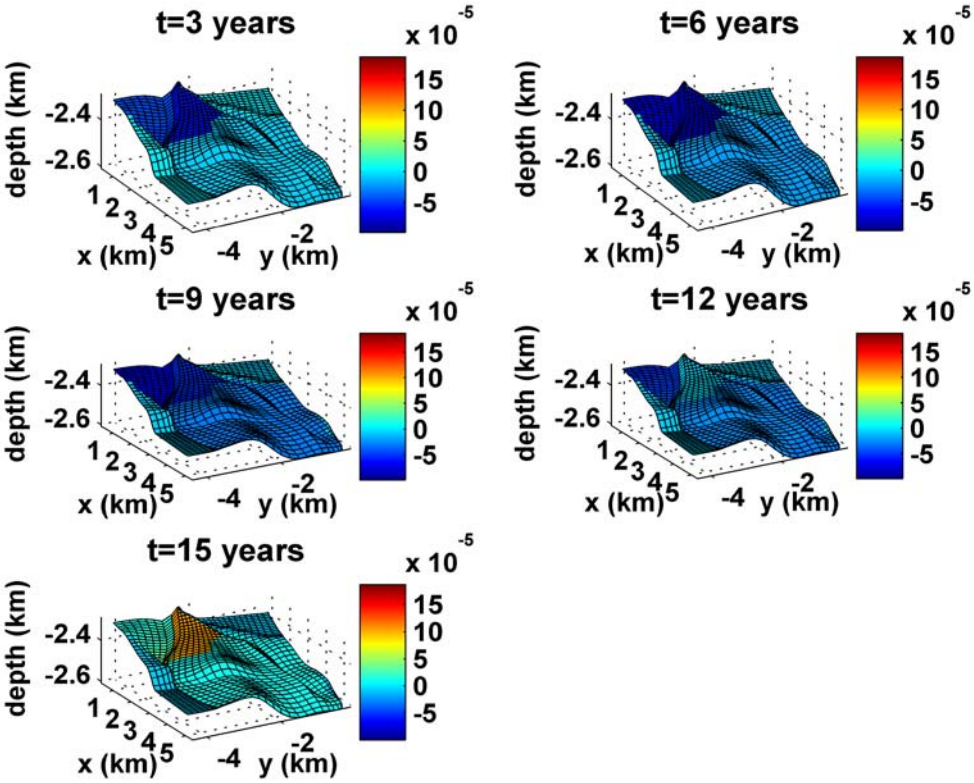

Fig. 4 Difference between m_D^{true} and m_D^{est}. Note that the main difference is located in the gas-bearing part of the model (for full analysis, see the main text)

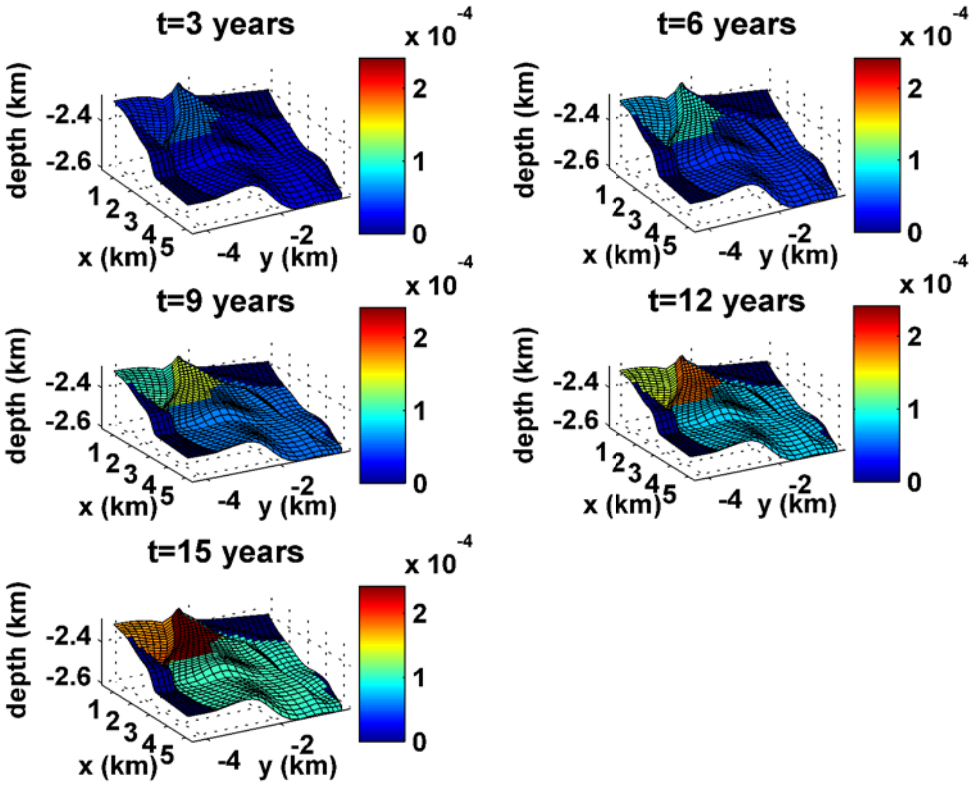

Fig. 5 Error estimates for m_D^{est} derived from the diagonal elements of the posterior covariance matrix

model still overestimates m_D^{true} for the initial time steps (3, 6, and 9 years of production), while underestimating it for the later time steps (12 and 15 years of production). The aquifer part of m_D^{est} differs from m_D^{true} only slightly ($\sim 0.5 \cdot 10^{-5}$), with no discernable trend over time. Only after 15 years of production is a slightly larger difference from m_D^{true} observed ($1 \cdot 10^{-5}$).

Given the probabilistic inversion approach adopted, the square root of the diagonal elements of the posterior covariance matrix can be interpreted as error estimates on the inverted model (Fig. 5). As expected, the errors increase through time, due to the accumulation of errors over all previous time steps. The largest errors are found for the gas-bearing part of the reservoir (up to $2.4 \cdot 10^{-4}$ (~25%) after 15 years of depletion). The extent to which the compaction field is defined more sharply can be seen from the reduction in the estimated errors. The errors decrease from 35% to 25% in the gas zone and from 79% to 13% in the aquifer. For the gas-bearing part of the reservoir, both the prior and the "true" models are within the error range of the inverted model estimate, but for the aquifer, only the "true" model is within the error range, and the prior model is not. In other words: in the aquifer, the adjustment achieved by the inversion leads to a range of possibilities that do not include the prior model.

4.2 Unraveling transmissibility and compaction coefficient

Having achieved the inversion of the subsidence information to compaction, the objective of this paper is to attempt to derive estimates of the uncertain compaction-driving parameters. As mentioned in Section 2, a full analysis of the relation between the driving parameters and surface subsidence is beyond the scope of the present paper, and our approach is simple, crude, and case-specific. This approach consists of four consecutive steps.

4.2.1 Step 1: Preliminary compaction coefficient estimate

Figure 6a shows the average pressure depletion in the aquifer (solid line) and gas-bearing layer (dashed line) vs the transmissibility of the models generated for the Monte Carlo simulations. Based on these relationships, we deduce that the sensitivity of the depletion in the gas-bearing parts of the reservoir to the transmissibility of the free water level is less than 23 bar (~11% of the maximum depletion), while the sensitivity of the depletion in the aquifer is over 137 bar (~85% of the maximum depletion). In order to derive an initial

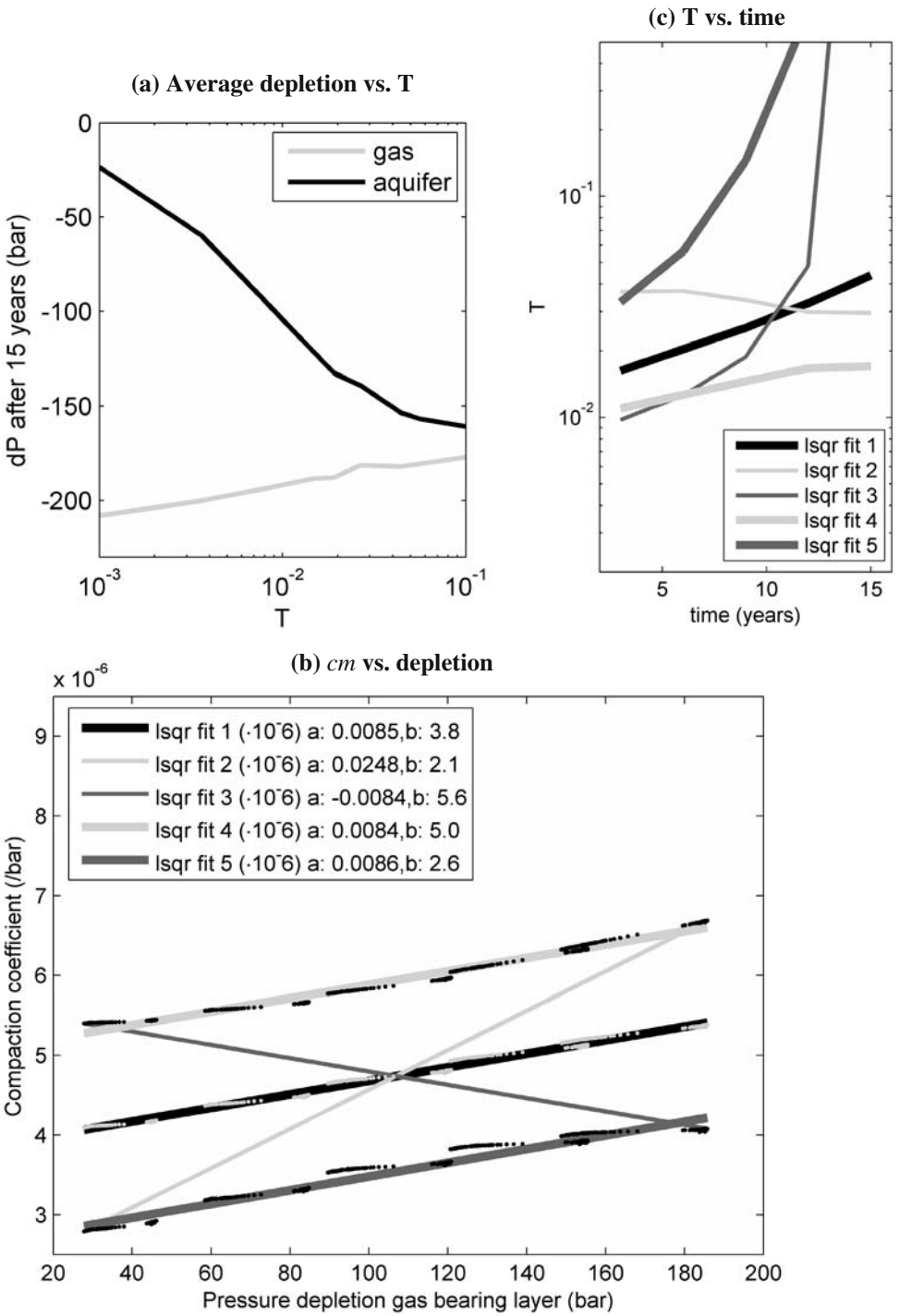

Fig. 6 **a** Average depletion in the aquifer (*black line*) and gas-bearing part (*gray line*) of the reservoir, plotted against their corresponding transmissibility of the Monte Carlo realizations. **b** Estimates of c_m for the gas-bearing elements of our model, plotted against their depletion (*light gray dots*). The corresponding error range is given by the *black dots*. A least-squares fit of a straight line to the c_m estimates allows an estimate of the depletion dependence of the compaction coefficient to be derived. In order to mimic the full coupled range of possible slopes and y-intercepts of the linear dependence on depletion, four additional least-squares fits are made. **c** Corresponding transmissibilities plotted vs time. Note that the estimates of the transmissibilities are not constant in time

estimate of the pressure dependence of the compaction coefficient, we rigorously assume that the effect of the transmissibility on the depletion in the gas-bearing layer is negligible (thus disregarding a maximum misfit of ∼11% for the smallest transmissibilities). With this assumption, c_m in the gas-bearing layer can be estimated by dividing m_D^{est} $(c_m \cdot dP)$ of the *inverted* model by the depletion (dP) in the gas-bearing part of the *prior* model:

$$c_m^{est,gas} \approx \frac{m_D^{est,gas}}{dP^{prior,gas}} \tag{4}$$

Figure 6b shows the resulting estimates of c_m of each gas-bearing element of the model plotted against the

corresponding prior pressure depletion (gray dots). The slope (a) and y-intercept (b) of the assumed linear depletion dependence of c_m can be derived by a least-squares fit of a straight line to these points. An error estimate on c_m can be derived in the same manner from a model obtained by adding/subtracting the error estimates deduced from the covariance matrix (Fig. 5) to the m_D^{est} (black dots Fig. 6b). To analyze the full coupled range of slopes and y-intercepts possible, we derive four least-squares fits in addition to the fit derived above (Fig. 6b).

4.2.2 Step 2: Derivation of corresponding transmissibilities

In the second step of our analysis, the transmissibilities for the aquifer depletions corresponding to the preliminary compaction coefficient estimates are derived at each time step.

In contrast to the gas-bearing part of the model, the depletion in the aquifer is significantly influenced by the transmissibility of the gas/water interface (~85%; Fig. 6a). Since the compaction coefficient is linearly dependent on the reservoir depletion, the dimensionless model (m_D) is related to the depletion by $m_D = a \cdot dP^2 + b \cdot dP$. Thus, the depletion in the aquifer grid cells of our dimensionless model can be computed through the positive solution of the quadratic equation:

$$dP_j = \frac{-b + \sqrt{b^2 + 4 \cdot a \cdot m_{D_j}^{est}}}{2a} \tag{5}$$

with a and b as calculated in step 1. For each preliminary compaction coefficient correlation (i.e., each set of a and b), the transmissibility at every time step of the model is calculated based on the average aquifer depletion at that time step ($\overline{dP}(a,b) = \frac{1}{n}\sum_j^n dP_j(a,b)$).

The resulting transmissibilities are shown in Fig. 6c. Immediately, we must conclude that our initial assumption of negligible influence of the transmissibility on the depletion in the gas-bearing zone was indeed invalid. For four of the five least-squares fits to the depletion-dependent compaction coefficients, the corresponding transmissibilities increase with time (Fig. 6c). Only the temporal behavior of the transmissibility corresponding to the fit with the largest slope and lowest y-intercept decreases in time. None of the fits are constant in time, even though this was prior knowledge that went into the prior covariance matrix. So, in order to derive estimates for all parameters that are consistent with our prior knowledge, we need to infer an estimate for $c_m(dP)$ that corresponds as closely as possible to a constant transmissibility in time. At the same time, the range of preliminary compaction coefficients spans an elliptical space bounding the feasible combinations of the slope and y-intercept of the compaction coefficient. Hence, the sought-after best estimates for the parameters correspond to the smallest minimum in the temporal variance of the transmissibility located within this bounding ellipse.

4.2.3 Step 3: Temporal variance of the transmissibility

In order to obtain an estimate of the slope and y-intercept that minimizes the temporal variance of the transmissibility, the difference between the minimum and maximum values of T as a function of a and b is contoured (Fig. 7a). Again, these values of T are determined from the depletion corresponding to the inferred m_D^{est}, without taking the error bounds into account. The ellipse spanned by the slopes and y-intercepts of the four bounding least-squares fits is given in white. The temporal variance of T shows a clear main minimum and several secondary minima. The main minimum corresponds to the following coefficients: $a = 0.00219 \cdot 10^{-5}$ bar^{-2}, $b = 0.4241 \cdot 10^{-5}$ bar^{-1}, and $T = 0.0136 \pm 0.0004$. However, these coefficients are outside our bounding ellipse. A secondary minimum with the coefficients $a = 0.00209 \cdot 10^{-5}$ bar^{-2}, $b = 0.292 \cdot 10^{-5}$ bar^{-1}, and $T = 0.0246 \pm 0.0010$ is located within our bounding ellipse. The temporal variance of the transmissibility in this minimum is a little more than twice the temporal variance of the main minimum.

4.2.4 Step 4: Compliance with inferred model

The coefficients of the minima must also result in a dimensionless model which complies with the inverted m_D^{est}. Therefore, the compliance of the dimensionless model estimates resulting from the secondary minimum with the inverted m_D^{est} is investigated by computing the difference between these models. It is found that the secondary minimum, which was located within the bounding ellipse, does indeed result in a dimensionless model that fits the inferred m_D^{est} within its error range. In comparison, the main minimum (located outside the bounding ellipse) leads to a difference from the inferred model that is more than twice its error estimate. Clearly, the transmissibility of the inverted model has gained a significant temporal dependence.

The reason a larger temporal variance in transmissibility is needed is because there is coupling between the compaction coefficient and the transmissibility that originates in the inversion process. The inversion procedure utilized does not take the individual contributions of the driving parameters to the reservoir

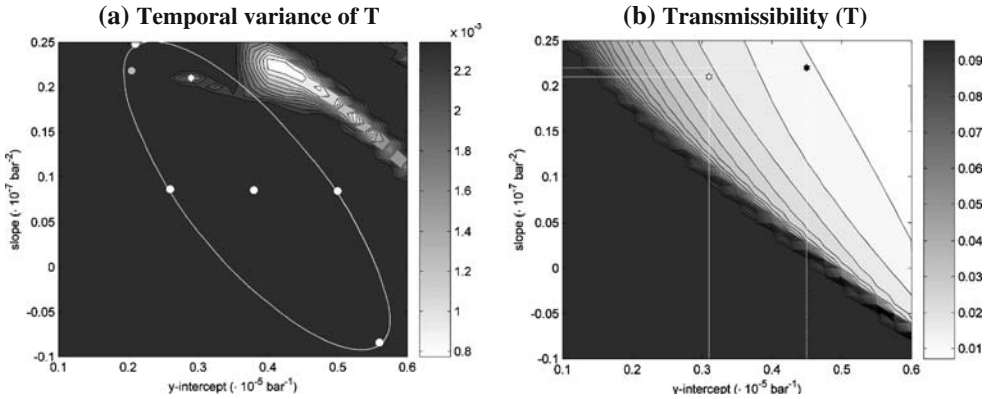

Fig. 7 **a** Temporal variance of the transmissibility as a function of the slope and y-intercept of the compaction coefficient. The *white dots* indicate the coefficients corresponding to the five least-squares fits of Fig. 6b. The bounding ellipse, which spans the full coupled range of slopes and y-intercepts, is also indicated in *white*. The *white star* indicates the secondary minimum for which the slope and y-intercept of the compaction coefficient are located within the bounding ellipse and properly agree with m_D^{est} and the least temporal variance in the transmissibility. **b** The transmissibility as a function of the slope and y-intercept of the compaction coefficient. Coupling between the parameters has been introduced into the inversion, which has led to the transmissibility becoming dependent on the compaction coefficient. The *black star* denotes the coefficients corresponding to the main minimum. The *white star* denotes the coefficients corresponding to the secondary minimum

compaction into account when deriving a model estimate of reservoir compaction. As a result, there is coupling between the parameters in the inverted compaction model. Thus, the temporal effect of the compaction coefficient contaminates the time-independent behavior of the transmissibility. The coupling between the parameters becomes clear in Fig. 7b, which shows the average estimate of T ($\overline{T}$) as a function of a and b. Clearly, the estimate of the transmissibility is now dependent on both the slope (a) and y-intercept (b) of the compaction coefficient.

4.2.5 Derivation of error bounds

Following the same procedure, bounding estimates for the compaction coefficient and transmissibility are derived by either adding (or subtracting) the error estimates to (or from) the inferred m_D^{est} (see Fig. 8 and Table 3). These estimates are based on the secondary minimum derived above. The minimum shifts in response to the addition or subtraction of the error estimates: it shifts to smaller slopes (less sensitivity to pressure) when m_D^{est} is chosen closer to the upper bound; it shifts to larger slopes and smaller intercepts when m_D^{est} is chosen closer to the lower bound. This is reflected in the values derived for the slope and y-intercept (Table 3).

The true values of the transmissibility (0.0337) and slope of the compaction coefficient ($0.0022 \cdot 10^{-5}$ bar^{-2}) lie within the uncertainty range of these parameters for the inverted model, but the prior values (0.0106 and $0 \cdot 10^{-5}$ bar^{-2}) do not. For the y-intercept of the linear dependence of the compaction coefficient on the pressure depletion of the reservoir, we find that neither the prior nor the true values of the parameter ($0.5 \cdot 10^{-5}$ bar^{-1} and $0.2 \cdot 10^{-5}$ bar^{-1}, respectively) are included in its derived error range. The derived range is in between the prior and true values, though significantly closer to the true value ($\sigma_{prior} = 0.203 \cdot 10^{-5}$ vs $\sigma_{true} = 0.05 \cdot 10^{-5}$).

4.2.6 Discussion

It is highly undesirable that the actual value of one of the parameters is not part of its error bound derived in the parameter estimation procedure. In practice, the only conclusion we might draw is that the compaction coefficient is in some way dependent on the depletion; however, no conclusion should be drawn on the degree of this dependence. This result is, of course, greatly influenced by the approach we followed. An 11% error was induced by our initial assumption that the effect of the transmissibility on the depletion in the gas-bearing layer is negligible. This assumption would be unnecessary in a proper parameter estimation procedure (Markov Chain Monte Carlo, data assimilation) and may shift or even tilt the location of our ellipse. Note, however, that the true parameter values are located within our bounding ellipse and, hence, are not unfeasible. They do require significantly more coupling between the parameters. Consequently, our assumption of a minimal temporal variance may be erroneous. Actually, the true parameter values correspond to a temporal variance in transmissibility of 0.0455 (grey dot

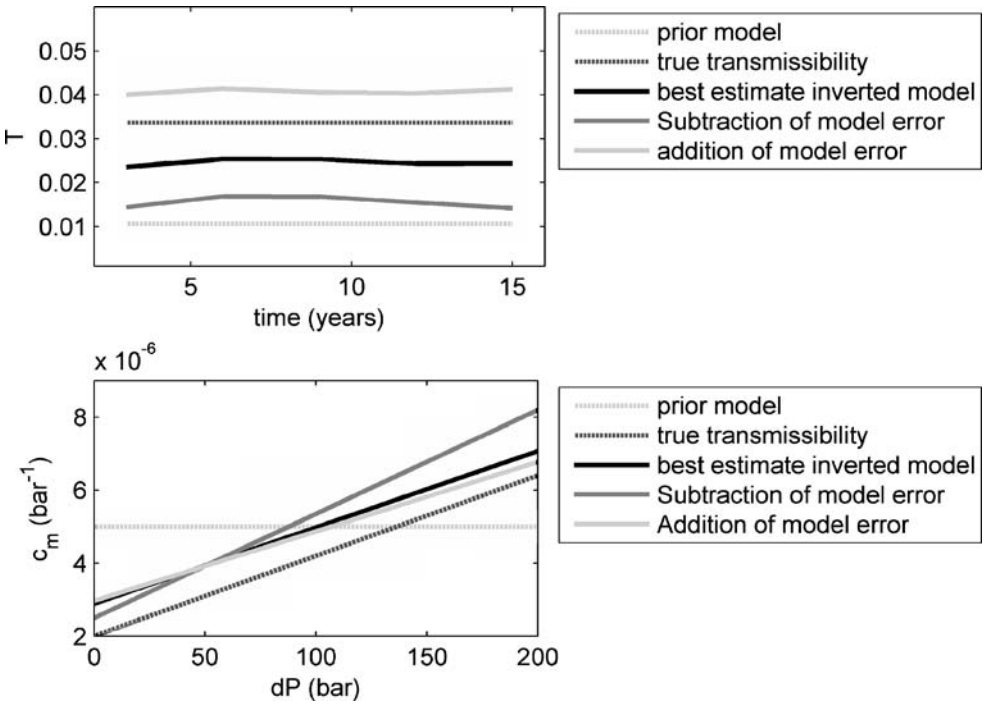

Fig. 8 *Top*: best estimate of the (near) constant transmissibility and its estimates when the model error is added and when it is subtracted. *Bottom*: best estimates of the depletion dependence of the compaction coefficient and its estimates when the model error is added and when it is subtracted

in Fig. 7a), which is more than 100 times larger than the temporal variance of the main minimum and 40 times larger than the temporal variance of our best estimate secondary minimum.

The coupling is a mathematical artifact of the inversion procedure and is not related to any physical process in the reservoir. The amount of coupling can be reduced by significantly increasing the amount of realizations utilized to compute the model covariance matrix. This increase in the amount of realizations will better define the model correlations in space and time and subsequently improve the discriminating power of the method. However, the total amount of realizations necessary for computing the model covariance matrix is given by $(n_{real})^{n_{par}}$, where n_{real} is the amount of realizations spanning the range of uncertainty of each parameter and n_{par} is the number of uncertain parameters. So, increasing the amount of realizations spanning the range of uncertainty of each parameter (n_{real}) may quickly lead to an unmanageable amount of models defining the model covariance matrix (especially if the amount of uncertain parameters increases as well). Therefore, a careful consideration of the objective of the inversion procedure (identification of depletion pattern or constraining driving parameters) is required prior to application in order to identify the scope of the MC analysis. The formal integration of subsidence in history-matching problems based on data assimilation is part of ongoing research at TNO.

4.3 Sensitivity to data accuracy

In order to test the robustness of our inversion procedure on the accuracy of the data, we modified the

Table 3 Overview of the deduced best estimates and their error range for the transmissibility and the slope and y-intercept of the compaction coefficient for all inverted models

	Model estimate			White noise added		
	T	Slope (10^{-7}) bar^{-2}	y-Intercept (10^{-5}) bar^{-1}	T	Slope (10^{-7}) bar^{-2}	y-Intercept (10^{-5}) bar^{-1}
Prior	0.0106	0	0.5	0.0106	0	0.5
True	0.0337	0.22	0.2	0.0337	0.22	0.2
Min	0.0153	0.285	0.250	0.0130	0.246	0.328
Best	0.0246	0.209	0.289	0.0243	0.194	0.315
Max	0.0406	0.190	0.297	0.0419	0.180	0.314

The "min" values are fits to the model estimate minus the error estimate, while the "max" values are fits to the model estimate plus the error estimate

data by adding random white noise. The white noise has a Gaussian distribution, with its mean at 0 and a standard deviation of 0.002 m. We find the difference from the previous inversion solution to be very small. The difference is mainly concentrated in the gas-bearing part of the model (difference <5% of the initial model estimate, compared to <1% of the initial model estimate for the aquifer). This indicates that our inversion procedure is quite robust and that significant inaccuracy in the data has only a slight influence on the inverted model estimate. However, this slight difference between the estimates might be significant if it is related to the uncertain parameters driving the dynamic reservoir compaction.

The estimates of the transmissibility and compaction coefficient we deduce from this solution are given in Table 3. The best estimate for the transmissibility is slightly lower (0.0003) than the estimate for the model without the white noise added, with a slightly larger error range. Consistent with our previous findings, the "true" model transmissibility lies within the error range deduced, while the prior model transmissibility does not. The estimates of the slope of the compaction coefficient are slightly lower than our earlier estimates ($\Delta a = 0.00015 \cdot 10^{-5}$ bar^{-2}), while the estimates for the y-intercept are larger ($\Delta b = 0.026 \cdot 10^{-5}$ bar^{-1}). As for the transmissibility, the slope of the "true" model is still included in the error range and the prior slope is not. Neither the y-intercept of the "true" model nor the y-intercept of the prior model is included in its error range. However, the misfits between the estimates of our model with white noise added to the data and the values of the "true" model are larger than those for our model without white noise. This demonstrates that the derivation of the parameters driving the dynamic reservoir compaction is sensitive to the accuracy of the data.

5 Conclusions

In this paper, we have investigated the possibility of utilizing the reservoir compaction model inferred from subsidence information to distinguish the characteristics of several compaction-driving parameters. The results demonstrate that the inversion procedure is capable of identifying temporal behavior in driving parameters, despite a time-independent prior. This capability originates in the incorporation of all spatial and temporal correlations imposed by the geology and reservoir data in the prior model covariance matrix. However, the inversion of subsidence data to reservoir compaction does lead to coupling between the various driving parameters. This becomes apparent in the dependency of the posterior transmissibility on the slope and y-intercept of the posterior compaction coefficient (Fig. 7b). This coupling is a direct consequence of the fact that the inversion procedure does not explicitly discriminate between the contributions of the driving parameters in its estimation process.

The assessment of the parameter estimates was based on a simple and crude unraveling procedure. Since the "true" value of one of the parameters is not included within the resulting error bound, we conclude that, at present, we are unable to derive proper estimates for the driving parameters - probably because of the assumptions made in the unraveling procedure (the negligible effect of T on the dP of the gas-bearing part of the reservoir and the minimization of the temporal variance of T; see Section 4.2.6). By incorporating subsidence data in a parameter estimation procedure (Markov chain Monte Carlo, data assimilation), these assumptions will become redundant and adequate estimate ranges for the parameters may be identified. This formal integration is being investigated in ongoing research.

Appendix

Derivation of prior model and prior model covariance

The characteristics of the model, including the depth of the free water level, are assumed to be known. The prime uncertainties in the reservoir simulation are the constant transmissibility of the gas/water interface and the depletion-dependent compaction coefficient. We adopt the Monte Carlo approach of simulating the depletion for 10 pseudo-random transmissibilities between 0.001 and 0.1 with a log-normal distribution centered at 0.01 and 10 pseudo-random compaction coefficients (see Table 2). A priori, it is not known whether the compaction coefficient is linearly dependent on the pressure depletion or whether it is independent of depletion. However, we stipulate that, after 15 years of production, the final compaction coefficient should be between $0.35 \cdot 10^{-5}$ and $0.75 \cdot 10^{-5}$ bar^{-1}, consistent with derivations made for the Rotliegend sandstones of the northern Netherlands [28].

Subsequently, all 100 models are arranged as rows in a matrix (**M100**) (thus, a column in this matrix represents the 100 different model values for a particular grid block at a particular time) and the prior model covariance matrix ($\mathbf{C}_m$) is computed. The variance values of the array columns of **M100** are arranged along

the diagonal of the covariance matrix; the remaining entries reflect the strength of the relationship between the grid blocks in both space and time. Thus, the Monte Carlo simulations simultaneously quantify the significant geological uncertainty in the transmissibility at the free water level and the compaction coefficient of the reservoir sandstone in the prior covariance matrix.

The prior model ($\mathbf{m}_0$) in the inversion method corresponds to the pressure depletion at mean transmissibility ($T = 0.0106$) and a constant compaction coefficient of $0.5 \cdot 10^{-5}$ bar^{-1}. This compaction coefficient is the commonly used average value for Rotliegend sandstone in the northern Netherlands [28], but it does not correspond to the mean of the Monte Carlo distribution (which is $c_m = (0.000962 \cdot dP + 0.375) \cdot 10^{-5}$ bar^{-1}). This is intentional, as the objective of this study is to emphasize the power of the inversion procedure to distinguish the depletion-dependent behavior of the compaction coefficient, based on temporal subsidence information.

References

1. Geertsma, J.: Land subsidence above compacting oil and gas reservoirs. J. Pet. Technol. **25**, 734–744 (1973)
2. van Opstal, G.H.C.: The effect of base-rock rigidity on subsidence due to reservoir compaction. In: Proc. 3rd Congr. Int. Soc. Rock Mech., vol. 2, pp. 1102–1111 (1974)
3. Fares, N., Li, V.C.: General image method in a plane-layered elastostatic medium. J. Appl. Mech. **110**, 781–785; Trans. ASME **55** (1988)
4. Morita, N., Whitfill, D.L., Nygaard, O., Bale, A.: A quick method to determine subsidence, reservoir compaction, and in-situ stress induced by reservoir depletion. J. Pet. Technol. **41**, 71–79 (1989)
5. Johnson, J.P., Rhett, D.W., Siemers, W.T.: Rock mechanics of the Ekofisk reservoir in the evaluation of subsidence. J. Pet. Technol. **41**, 717–722 (1989)
6. Hejmanowski, R.: Prediction of surface subsidence due to oil- or gasfield development. In: Proceedings of the Fifth International Symposium on Land Subsidence SISOLS95, The Hague, 16–20 October 1995
7. Fredrich, J.T., Deitrick, G.L., Arguello, J.G., DeRouffignac, E.P.: Reservoir compaction, surface subsidence and casing damage: a geomechanics approach to mitigation and reservoir management. SPE Eurock **46284**, 403–412 (1998)
8. Chin, L.Y., Thomas, L.K.: Fully coupled analysis of improved oil recovery by reservoir compaction. Paper presented at the SPE Ann. Tech. Conf. & Exhib., Houston, no. 56753 (1999)
9. Settari, A., Walters, D.A.: Advances in coupled geomechanical and reservoir modeling with applications to reservoir compaction. SPE J. **6**, 334–342 (2001)
10. Fokker, P.A., Orlic, B.: Semi-analytic modeling of subsidence. Math. Geol. **38**, 565–589 (2006)
11. Marchina, P.J.M.: The use of subsidence data to monitor reservoir behaviour. SPE **36918**, 413–421 (1996)
12. Carnec, C., Fabriol, H.: Monitoring and land subsidence at the Cerro Prieto geothermal field, Baja California, using SAR interferometry. Geophys. Res. Lett. **26**, 1211–1214 (1999)
13. Vasco, D.W., Karasaki, K., Doughty, C.: Using surface deformation to image reservoir characteristics. Geophysics **65**, 132–147 (2000)
14. Du, J., Olson, J.E.: A poroelastic reservoir model for predicting subsidence and mapping subsurface pressure fronts. J. Pet. Sci. Eng. **30**, 181–197 (2001)
15. Dusseault, M.B., Rothenburg, L.: Analysis of deformation measurements for reservoir management. Oil & Gas Sci. Tech, Rev. IFP **57**, 539–554 (2002)
16. Fokker, P.A.: Subsidence prediction and inversion of subsidence data. Paper presented at the SPE Rock Mechanics Conference, Irving, no. 78227 (2002)
17. Du, J., Brissenden, S., McGillivray, P., Bourne, S., Hofstra, P., Davis, E.-J., Roadarmel, W.H., Wolhart, S.L., Wright, C.A.: Mapping fluid flow in a reservoir using tiltmeter-based surface deformation measurements. Paper presented at the SPE Ann. Tech. Conf. & Exhib., Dallas, no. 96897 (2005)
18. Muntendam-Bos, A.G., Kroon, I.C., Fokker, P.A.: Time-dependent inversion of surface subsidence due to dynamic reservoir compaction. Math. Geosci. (2008). doi:10.1007/s11004-007-9135-3
19. Hettema, M., Papamichos, E., Schutjens, P.: Subsidence delay: field observations and analysis. Oil & Gas Sci. Tech. **57**, 443–458 (2002)
20. Merle, H.A., Kentie, C.J.P., van Opstal, G.H.C., Schneider, G.M.G.: The Bachaquero study – a composite analysis of the behavior of a compaction drive/solution gas drive reservoir. SPE JPT, 1107–1115 (1976, September)
21. Waal, J.A. de, Smits, R.M.M.: Prediction of reservoir compaction and surface subsidence: field application of a new model. Paper presented at the SPE Ann. Tech. Conf. & Exhib., Las Vegas, no. 14214 (1988)
22. McLendon, T.H.: Performance prediction for the M-6 area of the Tia Juana field using a rate-dependent pore volume compressibility model and extended material balance. Paper presented at the SPE Ann. Tech. Conf. & Exhib., Dallas, no. 22939, pp. 553–564 (1991)
23. Schutjens, P.M.T.M., Hanssen, T.H., Hettema, M.H.H., Merour, J., de Bree, P., Coremans, J.W.A., Helliesen, G.: Compaction-induced porosity/permeability reduction in sandstone reservoirs: data and model for elasticity-dominated deformation. Paper presented at the SPE Ann. Tech. Conf. & Exhib., New Orleans, no. 88441 (2004)
24. Lee, K.L.: Subsidence earthquake at a Californian oil field. In: Proc. Int. Conf. on Eval. and Pred. of Sub., Pensacola Beach, pp. 549–564 (1978)
25. Schroot, B.M., Fokker, P.A., Lutgert, J.E., Van Der Meer, B.G.H., Orlic, B., Scheffers, B.C., Barends, F.B.J.: Subsidence induced by gas production: and integrated approach. In: Land Subsidence, special volume, Proceedings of the Seventh International Symposium on Land Subsidence, pp. 79–99. Shanghai, 23–28 October 2005
26. Tarantola, A.: Inverse Problem Theory and methods for model parameter estimation. SIAM, Philadelphia (2005)
27. Dake, L. P.: Fundamentals of reservoir engineering. In: Developments in Petroleum Science, vol. 8, 443 pp. Elsevier Science, Amsterdam (1978)
28. Mobach, E., Gussinklo, H.J.: In-situ reservoir compaction monitoring in the Groningen field. SPE Eurock **28094**, 535–547 (1994)
29. Hower, T.L., Jones, R.E.: Predicting recovery of gas reservoirs under waterdrive conditions. Paper presented at the SPE Ann. Tech. Conf. & Exhib., Dallas, no. 22937 (1991)